A&A 433, L45–L48 (2005)
DOI: 10.1051/0004-6361:200500023

Astronomy & Astrophysics

INTEGRAL observation of V 0332+53 in outburst

I. Kreykenbohm[1,2], N. Mowlavi[2,3], N. Produit[2,3], S. Soldi[2,3], R. Walter[2,3], P. Dubath[2,3], P. Lubiński[4,2], M. Türler[2,3], W. Coburn[5], A. Santangelo[1], R. E. Rothschild[5], and R. Staubert[1]

[1] Institut für Astronomie und Astrophysik – Astronomie, Sand 1, 72076 Tübingen, Germany
[2] INTEGRAL Science Data Centre, 16 Ch. d'Écogia, 1290 Versoix, Switzerland
e-mail: Ingo.Kreykenbohm@obs.unige.ch
[3] Observatoire de Genève, Chemin des Maillettes 51, 1290 Sauverny, Switzerland
[4] N. Copernicus Astronomical Center, Bartycka 18, Warsaw 00-716, Poland
[5] Space Sciences Laboratory, University of California, Berkeley, Berkeley, CA, 94702-7450, USA
[6] Center for Astrophysics and Space Sciences, University of California at San Diego, La Jolla, CA 92093-0424, USA

Received 18 January 2005 / Accepted 9 February 2005

Abstract. We present the analysis of a 100 ks *INTEGRAL* (3−100 keV) observation of the transient X-ray pulsar V 0332+53 in outburst. The source is pulsating at $P_{\rm Pulse} = 4.3751 \pm 0.0002$ s with a clear double pulse from 6 keV to 60 keV. The average flux was ∼550 mCrab between 20 keV and 60 keV. We modeled the broad band continuum from 5 keV to 100 keV with a power-law modified by an exponential cut off. We observe three cyclotron lines: the fundamental line at $24.9^{+0.1}_{-0.1}$ keV, the first harmonic at $50.5^{+0.1}_{-0.1}$ keV as well as the second harmonic at $71.7^{+0.7}_{-0.8}$ keV, thus confirming the discovery of the harmonic lines by Coburn et al. (2005) in *RXTE* data.

Key words. X-rays: stars – stars: flare – stars: pulsars: individual: V0332+53 – stars: magnetic fields

1. Introduction

V 0332+53 (RA = $03^{\rm h}34^{\rm m}59\overset{\rm s}{.}89$, Dec = $+53°10'23\overset{''}{.}6$) is a recurrent transient X-ray pulsar. The system consists of the O8−9Ve star BQ Cam (Negueruela et al. 1999; Bernacca et al. 1984) and a neutron star (NS) in an eccentric ($e = 0.31$) 34.25 d orbit, spinning with a period of 4.375 s (Stella et al. 1985). Since its discovery by the Vela 5B satellite during an outburst in 1973 (Terrell & Priedhorsky 1984), the system has so far exhibited three more outbursts in 1983 (Tanaka 1983), 1989 (Makino 1989), and 2004. The peak luminosities during these outbursts were quite different: while the 1973 outburst reached 1.6 Crab (Negueruela et al. 1999), the flux of the 1983 outburst was about 10 times lower (Unger et al. 1992), and the 1989 outburst reached a flux of 0.4 Crab (Makishima et al. 1990). Based on a distance of 7 kpc (Negueruela et al. 1999), which places the source beyond the Perseus spiral arm in the outer arm of the galaxy, the maximum X-ray luminosity reached during the 1973 outburst was $L_{\rm X} > 10^{38}$ erg s^{-1} – close to the Eddington luminosity.

For the 1989 outburst observed by *Ginga* (Makishima et al. 1990), the X-ray spectrum has been modeled by a power-law plus a high energy cut off . The analysis further revealed a deep and broad absorption line at 28.5 keV which was interpreted as a cyclotron resonant scattering feature (CRSF). The 1989 data also revealed the presence of a quasi periodic oscillation (QPO) with a centroid frequency of 0.05 Hz (Takeshima et al. 1994). The source furthermore exhibits aperiodic short term variability similar to Cygnus X-1 (Stella et al. 1985).

The optical companion BQ Cam was observed to brighten from January 2002 on by Goranskij & Barsukova (2004). Since a similar brightening had been observed to precede the two previous X-ray outbursts, they predicted an outburst of V 0332+53 within the next one or two years. Indeed, the source entered an outburst in November 2004, after almost 15 years of quiescence, recorded by the All-Sky Monitor (*ASM*, Swank et al. 2004) onboard the Rossi X-ray Timing Explorer (*RXTE*). The X-ray flux increased continuously and reached 1 Crab in the 2−12 keV band in 2004 December (Remillard 2004). Subsequent pointed observations with *RXTE* revealed the presence of three cyclotron lines, at 26.34 ± 0.03 keV, 49.1 ± 0.2 keV, and 74 ± 2 keV (Coburn et al. 2005).

In this Letter, we report on the 3−100 keV analysis based on the observation of V 0332+53 performed on 2005 January 6−10 by the *INTEGRAL* satellite. We describe the *INTEGRAL* observations in Sect. 2. Imaging, spectral, and timing analysis are presented in Sect. 3, and summarized in Sect. 4.

2. *INTEGRAL* observations

Although the peak of the outburst of V 0332+53 was reached in 2004 December, a dedicated target of opportunity (TOO) observation could not be scheduled before 2005 January 5 due to satellite orientation constraints relative to the Sun. 100 ks

of good data were recorded for V 0332+53 between January 6 and 10−30 ks in staring mode in revolution 272 (pointing 75 on January 6th 08:47:45−18:14:00 UT), 50 ks in hexagonal mode in revolution 273 (pointings 66 to 82 from January 8 at 22:18:12 to 9th at 15:45:47 UT), and 20 ks in hexagonal mode in revolution 274 (pointings 4 to 9 on January 10 from 03:20:30 to 09:22:11 UT). V 0332+53 was always in the field of view (FOV) of all three high energy instruments.

3. Data analysis

We analyzed data from all instruments on board *INTEGRAL*. The X-ray instrument JEM-X provides data in the 2−30 keV energy band. The ISGRI layer of the imager IBIS covers the 20−800 keV band with an imaging resolution of 2 arcmin and about 10% energy resolution at 20 keV. The PICsIT layer provides data above 200 keV. The spectrometer SPI provides high energy resolution (1 keV below 100 keV) in the 20 keV to 8 MeV energy range. The optical monitoring camera (OMC) provides the magnitude in the *V*-band for selected optical targets.

Imaging, spectral, and timing analyses were performed using version 4.2 of the Offline Scientific Analysis (OSA) package as described in the cookbooks available with the OSA.

3.1. Image analysis

The analysis of V 0332+53 is facilitated by the fact that it is the only bright X-ray source in the FOV. The mean flux during the three observations is about 550 mCrab in the 20−60 keV energy band in *ISGRI* and 700 mCrab in the 3−10 keV energy band in JEM-X, consistent with *RXTE*/*ASM*. The flux at 20 keV during these observations is similar to that measured in December 2004 during the Galactic Plane Scan (Turler et al. 2004). We note that, at lower energies, the *RXTE*/*ASM* has recorded a steady decline of the 3−10 keV flux from a peak value of ∼1 Crab at the end of 2004 December to ∼0.6 Crab at the time of the *INTEGRAL* observation, the latter value being consistent with the JEM-X observation.

The source was not detected by PICsIT; this is actually not surprising, knowing that the spectra of accreting X-ray pulsars are exponentially falling at higher energies, making them difficult to detect above 100 keV (see, e.g., Coburn et al. 2002).

The OMC observed the optical companion of V 0332+53, BQ Cam at $M_V \sim 15.4 \pm 0.2$ consistent with simultaneous ground based observations (Masetti et al. 2005). The observations confirm that BQ Cam is in an excited state.

3.2. Spectral analysis

We combined all data to obtain a spectrum with a very high signal to noise ratio. Spectra of accreting X-ray pulsars are, however, notoriously difficult to fit, especially if CRSFs are involved. Special care has also to be taken that no artificial residuals are introduced by the model (as is the case for, e.g., the broken power law and/or the high energy cut off, cf. Kreykenbohm et al. 1999). We used the `cutoffpl` model of *XSPEC* which describes the overall shape of the continuum reasonably well (see Fig. 1). We fit JEM-X and ISGRI data simultaneously applying only a constant to allow for a free normalization between the two instruments. A systematic error of 2% has been applied to account for the uncertainties of the response matrices of JEM-X and ISGRI. We did not use SPI as the fit is completely dominated by the ISGRI instrument above 20 keV anyway. For comparison, however, we also show the SPI data in Fig. 1a, which shows the CRSFs at the same energies as ISGRI.

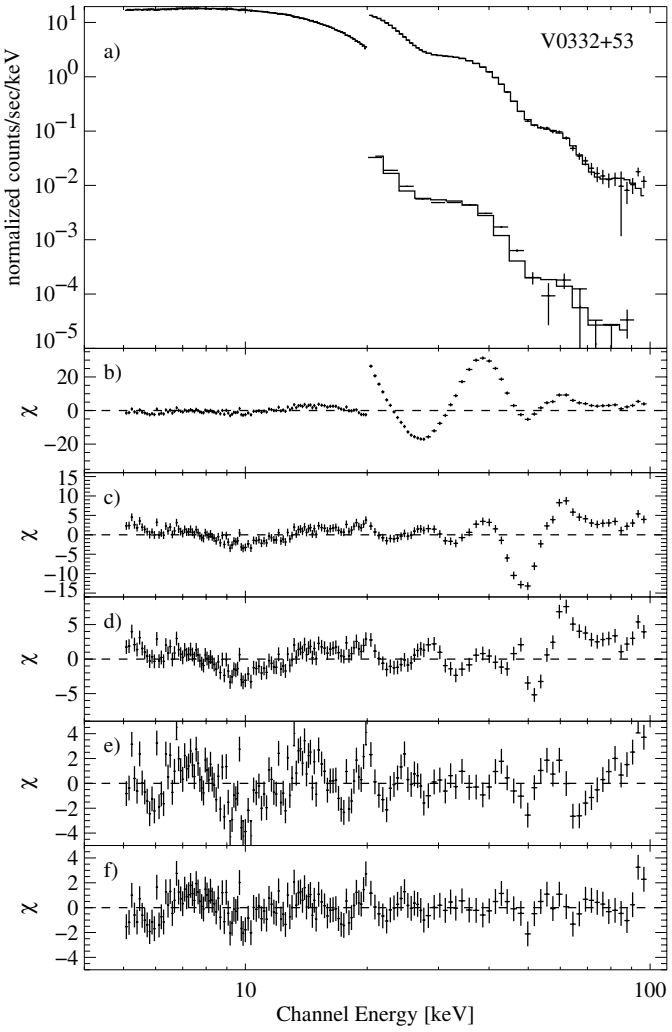

Fig. 1. a) Combined spectrum and model of data obtained with JEM-X (*left*), ISGRI (*upper right*), and SPI (*lower right*). Note that SPI is only shown for comparison, but is not used for the fits below. The dips of the cyclotron lines are already very apparent in the raw data. The continuum is modeled with the `cutoffpl` model; **b)** model without any Gaussian lines applied; in **c)** one Gaussian at $26.6^{+0.1}_{-0.1}$ keV is included; in **d)** another Gaussian is included at $47.1^{+0.1}_{-0.2}$ keV; **e)** a third Gaussian is included $30.8^{+0.3}_{-0.1}$ keV (see Table 1) resulting in a much better description of the spectrum between 20 keV and 40 keV, but significant deviations remain above 50 keV; **f)** the best fit using a fourth Gaussian at $71.7^{+0.7}_{-0.8}$ keV results in small residuals also at high energies. Note that all parameters mentioned previously are for the respective preliminary fits only. See Table 1 for the parameters of the final fit.

While the `cutoffpl` model fits the low energy data reasonably well without any photoelectric absorption, large absorption line-like structures are present above 20 keV.

Table 1. Fitted parameters from phase averaged spectra using JEM-X and ISGRI spectra. All errors represent 90% confidence.

Parameter		2 CRSFs	3 CRSFs
Γ		$-0.46^{+0.01}_{-0.01}$	$-0.20^{+0.01}_{-0.01}$
$E_{\rm Cut}$	[keV]	$6.5^{+0.1}_{-0.1}$	$8.0^{+0.1}_{-0.1}$
$E_{\rm Cyc,1a}$	[keV]	$25.2^{+0.1}_{-0.1}$	$24.9^{+0.1}_{-0.1}$
$\sigma_{\rm Cyc,1a}$	[keV]	$2.9^{+0.1}_{-0.1}$	$2.4^{+0.1}_{-0.4}$
$\tau_{\rm Cyc,1a}$		$1.25^{+0.01}_{-0.01}$	$0.74^{+0.01}_{-0.02}$
$E_{\rm Cyc,1b}$	[keV]	$30.8^{+0.3}_{-0.1}$	$29.0^{+0.1}_{-0.2}$
$\sigma_{\rm Cyc,1b}$	[keV]	$3.7^{+0.2}_{-0.1}$	$5.0^{+0.1}_{-0.1}$
$\tau_{\rm Cyc,1b}$		$0.81^{+0.02}_{-0.08}$	$1.28^{+0.01}_{-0.01}$
$E_{\rm Cyc,2}$	[keV]	$50.1^{+0.1}_{-0.1}$	$50.5^{+0.1}_{-0.1}$
$\sigma_{\rm Cyc,2}$	[keV]	$7.1^{+0.1}_{-0.3}$	$8.1^{+0.1}_{-0.2}$
$\tau_{\rm Cyc,2}$		$1.58^{+0.03}_{-0.01}$	$2.33^{+0.03}_{-0.02}$
$E_{\rm Cyc,3}$	[keV]	–	$71.7^{+0.7}_{-0.8}$
$\sigma_{\rm Cyc,3}$	[keV]	–	$6.3^{+0.5}_{-0.4}$
$\tau_{\rm Cyc,3}$		–	$1.8^{+0.5}_{-0.4}$
χ^2	(D.O.F.)	230.2 (147)	170.4 (144)

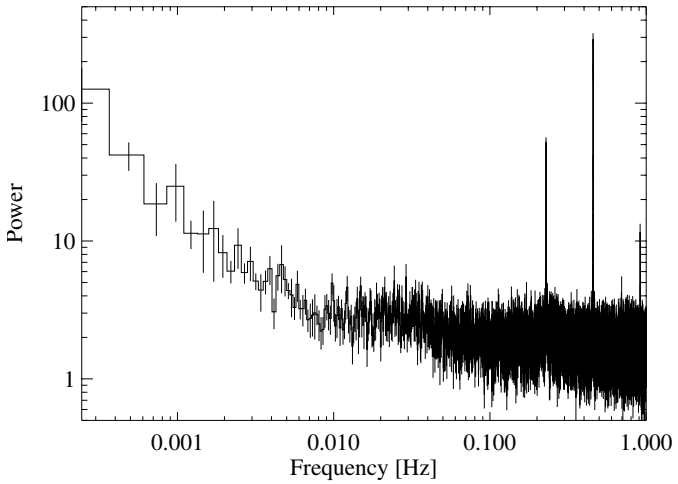

Fig. 2. Power spectrum of the 50 ks observation in revolution 273 of V 0332+53 (see Sect. 2). The smaller peak at 0.22 Hz (4.375 s) is due to the pulse period while the higher peak at 0.45 Hz (2.188 s) is due to the double-peaked pulse profile of V 0332+53 (see Fig. 3).

The observation of harmonically spaced lines confirms that these features originate from cyclotron resonant scattering. We use a multiplicative Gaussian absorption line at $E_{\rm C} = 26.5^{+0.1}_{-0.1}$ keV to fit the strong fundamental CRSF between 20 keV and 30 keV (discovered by Makishima et al. 1990). At ∼50 keV the first harmonic CRSF (discovered by *RXTE*, Coburn et al. 2005) is also extremely well detected (see Fig. 1c). After fitting both CRSFs, many residuals still remain. This is due to the non-Gaussian shape of the fundamental, as observed by Mihara (1995) in the *Ginga* data and Coburn et al. (2005) in *RXTE* data. Using Lorentzian instead of Gaussian absorption lines does not improve the fit. To model the fundamental, we use a pair of Gaussians at $25.2^{+0.1}_{-0.1}$ keV and $30.8^{+0.3}_{-0.1}$ keV. The significant residuals visible at ∼70 keV (see Fig. 1e) are identified with the second harmonic CRSF (discovered by Coburn et al. 2005). They are fitted with a Gaussian at $E = 71.7^{+0.7}_{-0.8}$ keV (see Fig. 1f). While the reported parameter values are for the respective preliminary fits, the final fit parameters are given in Table 1.

To further check the validity of our results, we used other spectral models to fit the data including the Negative Positive EXponential (NPEX, Mihara 1995). In all cases, we found that three CRSFs are present, although the actual line parameters depend on the shape of the continuum. We also note that the CRSFs observed at 25 keV and 50 keV are much more significant than the deviations known to be present in the OSA 4.2 response matrix or the energy calibration of ISGRI between 20 keV and 50 keV; hence we are confident that the spectral behavior is dominated by the source and not by calibration issues.

3.3. Timing analysis

To determine the period of the pulsar we barycentered the event arrival times for ISGRI and JEM-X and derived power spectra with the *xronos* package for each of the three parts of the observation (see Sect. 2). No correction for orbital motion has been applied since the uncertainties of the ephemeris (Stella et al. 1985) are too large to extrapolate over 20 years and the derivation of a new ephemeris is out of the scope of this Letter.

Two periodicities are clearly detected in the power spectrum (see Fig. 2): one peak at 0.2286 Hz associated with the spin of the NS and one at half period due to the double-peaked pulse profile. The derived pulse periods are 4.3753 ± 0.0001 s (Rev. 272), 4.37501 ± 0.00006 s (Rev. 273), and 4.3749 ± 0.0002 s (Rev. 274). These variations are compatible with the effect expected from the orbital motion.

We created pulse profiles in several energy bands. While the pulse profile for Rev. 272 and 273 exhibits a clear double pulse at all energies, two behaviors are distinguishable in the pulse profile for Rev. 274: below 6 keV only one pulse is detected, while two peaks are clearly observable at all energies above 6 keV (see Fig. 3). The secondary pulse is at a level of 60% to 75% amplitude of the main pulse (after subtracting the non-pulsed flux). At the same time, the pulsed fraction increases from 13% in 3−15 keV to 22% in 15−30 keV and 35% in 30−60 keV.

We also performed rudimentary phase resolved spectroscopy by deriving ISGRI spectra for the main pulse, the secondary pulse, and the pulse minimum using data from one pointing in Rev. 274. The normalized ratio between these spectra is consistent with unity between 20 keV and 45 keV, i.e., the spectrum in this energy range does not vary over the pulse. Above 45 keV the statistics are not sufficient from one pointing. More detailed pulse phase resolved spectroscopy requires a valid ephemeris to correct for the binary motion.

4. Summary

V 0332+53 is only the second X-ray source known so far that exhibits at least three CRSFs; the other object, 4U 0115+63, exhibits five lines (Coburn et al. 2004). All three CRSFs in

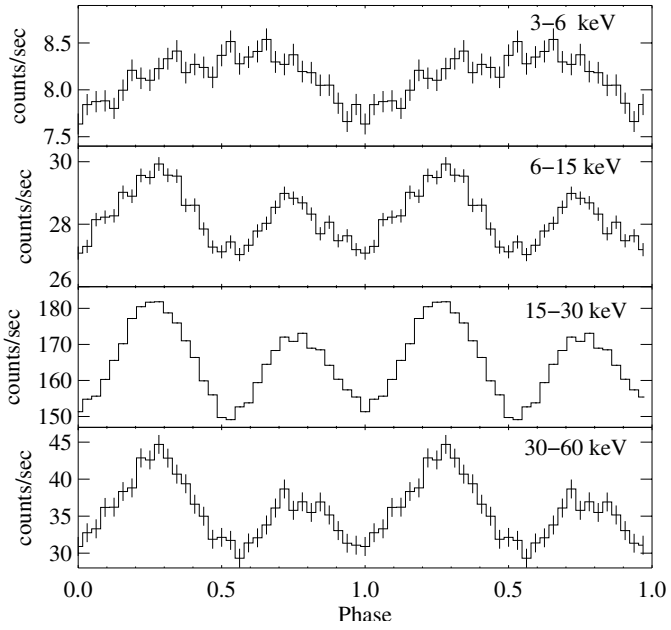

Fig. 3. Lightcurve of V 0332+53 in two JEM-X and two ISGRI energy bands in Rev. 274 (see Sect. 2) folded with $P_{\rm Pulse} = 4.37492$ s. Note the change of the pulse profile at low energies.

the *INTEGRAL* data are located close to those energies derived from *RXTE*. The fundamental CRSF has resolved structure such that even two Gaussian lines are barely able to fit it. Comparing line shapes derived from pulse phase resolved spectra to Monte Carlo simulations of Araya & Harding (1999) would allow one to infer constraints on the geometry of the emission region. Such a study will be presented in a forthcoming paper. To derive the strength of the magnetic field, we need to derive the "true" centroid energy of the fundamental, which is difficult to obtain. The first harmonic at 50 keV, however, is fit by a single Gaussian with small residuals (see Fig. 1). Assuming that the coupling factor between the fundamental and the first harmonic is indeed 2.0, we derive an energy for the fundamental of 25.3 ± 0.1 keV, compatible with the centroid energy of the lower of the two Gaussians used to fit the 25 keV feature. If we therefore assume that the energy of the fundamental CRSF is indeed 25.3 keV, that the NS has the canonical mass of $1.4\,M_{\odot}$, and that the CRSFs originate close to surface of the NS we infer a strength of the magnetic field of $B = (1+z)/11.6 \times E_{\rm Cyc} \times 10^{12}\,{\rm G} \approx 2.7 \times 10^{12}\,{\rm G}$ with a gravitational redshift z of 0.25. The coupling factor between the fundamental CRSF and the second harmonic is 2.85 ± 0.05, slightly smaller than the theoretical 3.0. The same has been observed for 4U 0115+63, where the shape of the fundamental line is also strongly distorted from that of a single Gaussian and the coupling factors are smaller than expected and is probably due to relativistic effects (Heindl et al. 1999; Santangelo et al. 1999).

The derived pulse period is almost identical to the period of the 1983 outburst (during which $P = 4.3753 \pm 0.0001$, Stella et al. 1985), indicating that the pulse period has, within the uncertainties arising from the lack of orbital correction, not changed significantly since 1983.

The behavior of the source seems to be different below and above 6 keV. The pulse profile exhibits two peaks at all energies from 6 keV to 60 keV, similar to other accreting X-ray pulsars (e.g., Vela X-1, Kreykenbohm et al. 1999), while it exhibits only one peak below 6 keV in Rev. 274 and two peaks in Rev. 272 and 273. The behavior is different from the 1983 outburst, where the secondary pulse was only present at very low energies (<5 keV, Stella et al. 1985). These authors also noticed a luminosity dependence of the pulse profile below 10 keV, two peaks being detected at higher luminosities and only one at lower luminosities. During the *INTEGRAL* observation, the average luminosity in the 20–60 keV band was ~550 mCrab – a high luminosity state according to Stella et al. (1985), but we see a more complex behavior with one peak below 6 keV and two peaks above 6 keV in Rev. 274. The strength of the secondary peak is still 60% of the main peak between 30 keV and 60 keV. Unfortunately, the statistics are not sufficient to determine a pulse profile at higher energy bands. Further analysis is in progress and will be reported in a forthcoming paper.

Acknowledgements. I.K. acknowledges DLR grants 50 OG 9601 and 50 OG 0501 and PL KBN grants 1P03D01827, PBZ-KBN-054/P03/2001, and 4T12E04727. R.E.R. acknowledges the support of NASA contracts NAS5-30720, grants NAG-12957 and NNG04GJ68G and of NSF international grants NSF_INT-9815741 and -0003773 for fostering the UCSD/Tübingen scientific collaboration.

References

Araya, R. A., & Harding, A. K. 1999, ApJ, 517, 334
Bernacca, P. L., Iijima, T., & Stagni, R. 1984, A&A, 132, L8
Coburn, W., Heindl, W. A., Rothschild, R. E., et al. 2002, ApJ, 580, 394
Coburn, W., Kalemci, E., Kretschmar, P., et al. 2004, ATel, 337, 1
Coburn, W., Kretschmar, P., Kreykenbohm, I., et al. 2005, ATel, 381, 1
Goranskij, V., & Barsukova, E. 2004, ATel, 245, 1
Heindl, W. A., Coburn, W., Gruber, D. E., et al. 1999, ApJ, 521, L49
Kreykenbohm, I., Kretschmar, P., Wilms, J., et al. 1999, A&A, 341, 141
Makino, F. 1989, IAU Circ., 4858, 1
Makishima, K., Mihara, T., Ishida, M., et al. 1990, ApJ, 365, L59
Masetti, N., Orlandini, M., Marinoni, S., & Santangelo, A. 2005, ATel, 388
Mihara, T. 1995, Ph.D. Thesis, RIKEN, Tokio
Negueruela, I., Roche, P., Fabregat, J., & Coe, M. J. 1999, MNRAS, 307, 695
Remillard, R. 2004, ATel, 371, 1
Santangelo, A., Segreto, A., Giarrusso, S., et al. 1999, ApJ, L85
Stella, L., White, N. E., Davelaar, J., et al. 1985, ApJ, 288, L45
Swank, J., Remillard, R., & Smith, E. 2004, ATel, 349, 1
Takeshima, T., Dotani, T., Mitsuda, K., & Nagase, F. 1994, ApJ, 436, 871
Tanaka, Y. 1983, IAU Circ., 3891, 2
Terrell, J., & Priedhorsky, W. C. 1984, ApJ, 285, L15
Turler, M., Di Cocco, G., Diehl, R., et al. 2004, ATel, 372, 1
Unger, S. J., Norton, A. J., Coe, M. J., & Lehto, H. J. 1992, MNRAS, 256, 725